Oxidation of Phosphine Donors to Phosphinimines via a Putative Fe-imido Intermediate

Jeremiah E. Stevens[a], Gillian P. Hatzis[a], Maria C. Seith[a], Curtis E. Moore[a], Christine M. Thomas[a,*]

[a]*Department of Chemistry and Biochemistry, The Ohio State University, 100 W. 18th Ave., Columbus, Ohio, 43210, United States*

**corresponding author: thomas.3877@osu.edu*

Abstract

The formation of Fe^{II} phosphinimine complexes by treatment of an *S* = 1 (PNNP)Fe^{II} complex with $MesN_3$ (Mes = 2,4,6-trimethylphenyl) is reported. The resulting compounds have been characterized structurally and spectroscopically. Zero-field ^{57}Fe Mössbauer spectroscopy and magnetic susceptibility measurements suggest a spin-state change occurs once both phosphines have been converted to phosphinmines, commensurate with the weaker field nature of phosphinimine ligands compared to phosphines. We propose that phosphine oxidation proceeds through nitrene transfer to Fe to afford a formally Fe^{IV}-imido intermediate that is more accurately predicted to have Fe^{III}-imidyl radical character. Although no such intermediate could be isolated due to its instability and rapid phosphine oxidation, we support this mechanistic proposal with stoichiometric experiments and *in silico* analyses at the *ω*B97X-D_3/def2-SVP level of theory. Our computational analyses confirm that the driving force for this transformation is very favorable.

Keywords: iron, phosphinimine, phosphine oxidation, organic azide, intramolecular nitrene transfer

Introduction

While early metal imido complexes have been ubiquitous in the literature for quite some time, reports of late metal imido complexes have only surfaced more recently. This can be attributed, in part, to the increased reactivity of such late metal imido complexes imparted by their higher *d* electron counts that lead to lower metal-ligand bond orders in certain geometries.[1,2] Iron imido complexes, specifically, are often invoked as intermediates in processes of both synthetic and biological importance.[3–5] For example, surface-bound iron imides are proposed as key intermediates in the industrial Haber-Bosch process[6] and nitrogen fixation by the nitrogenase enzyme and its synthetic mimics.[7,8] The reactions of terminal Fe=NR compounds include hydrogen atom transfer (HAT),[9–12] nitrene transfer[11,13,14] and [2+2] cycloaddition,[15] with synthetic applications in C–H bond amination,[16] aziridination,[17] alkyne carboamination,[18] and alkene transposition.[19]

While terminal Fe imido complexes containing phosphine donor ligands have been isolated and structurally characterized,[11,20–26] in many cases metal-bound phosphinimines are generated upon addition of organic azides to phosphine-bound Fe complexes (Figure 1). The resulting highly polar phosphinimine P–N bond has two resonance forms: a neutral ylene (R_3P=NR) and a zwitterionic ylide (R_3P^+–N^-R), resulting in a ligand with excellent σ- and π-donor abilities. [27] For example, Deng *et al.* observed formation of the phosphinimine by treatment of their bis(anilido)phosphine Fe^{II} complex with organic azides.[28] Deng proposes that this transformation proceeds through an Fe=NR intermediate, but such a complex was not isolated or observed. In another recent example, Szymczak and coworkers reported the oxidation of the appended phosphines of an Fe complex ligated by a 6,6'-phosphine-substited 2,2'-bipyridine ligand via treatment with an aryl azide.[29]

In this work, we show that the triarylphosphine donors of our previously reported tetradentate bis(amido)bis(phosphine)Fe^{II} complex (PNNP)Fe (**1**)[30] are converted to phosphinimines in a stepwise fashion by treatment with mesityl azide ($MesN_3$, Mes = 2,4,6-trimethylphenyl). Although we were not able to observe or isolate a putative Fe=NR intermediate, we provide computational and experimental support that a mechanism involving such an intermediate is plausible.

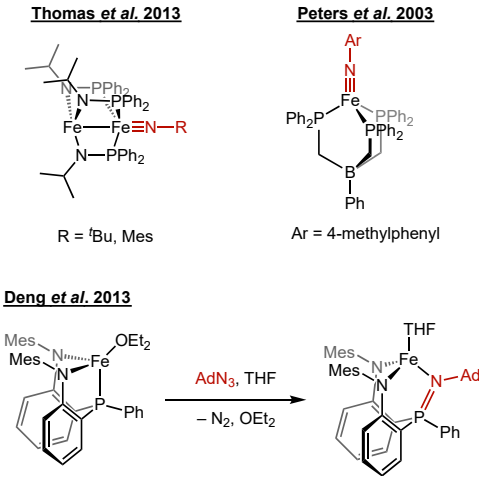

Figure 1: Selected examples of isolated iron imido complexes with bound phosphine ligands (top) and an example of reactivity of a phosphine-bound iron complex with organic azides (bottom).

Results and Discussion

Inspired by the prolific use of organic azides as nitrene transfer reagents, we sought to explore the generation of an Fe=NR imido species via oxidative group transfer from an organic azide to the square planar *S* = 1 (PNNP)Fe complex (**1**). The reaction of **1** with 1 equiv of $MesN_3$ (Scheme 1) in C_6H_6 resulted in a color change from red-brown to a deep orange color. The ^{1}H NMR spectrum of the resulting product is indicative of the formation of a new asymmetric paramagnetic product **2**, featuring 17 distinct resonances between 35 and –60 ppm (Figure S1, top). The increased number of resonances relative to the ^{1}H NMR spectrum of **1** suggests the disruption of at least one of the mirror planes of the (PNNP)Fe framework.

Orange single crystals of **2** suitable for X-ray diffraction analysis were obtained, and the solid-state structure of **2** (Figure 2) revealed an approximately square planar (τ_4 = 0.171)[31] complex with a MesN fragment inserted into one of the two Fe–P bonds of **1**. The P–N distance of 1.6201(17) Å is on the order of the average P=N double bond (1.584 Å) in structures deposited into the Cambridge Structural Database,[32] consistent with formal two-electron oxidation of the triarylphosphine from P^{III} to P^{V}. Also of note is the contraction of the Fe1–N2 linkage (1.8984(17) Å) *trans* to the newly-formed phosphinimine relative to the Fe1–N1 linkage (1.9659(18) Å) *trans* to the unfunctionalized phosphine, which demonstrates the weaker *trans* influence of the phosphinimine relative to the phosphine expected due to the phosphinimine's lack of π-accepting character.

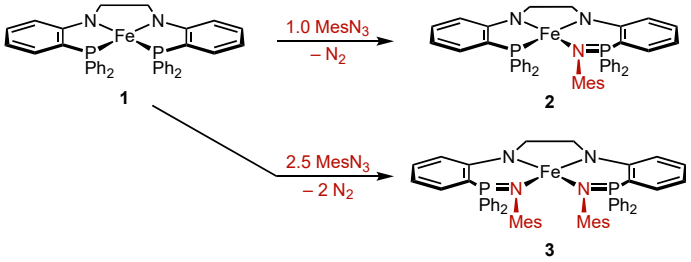

Scheme 1: Reaction of (PNNP)Fe (**1**) with 1 and 2.5 equiv mesityl azide to produce **2** and **3**, respectively.

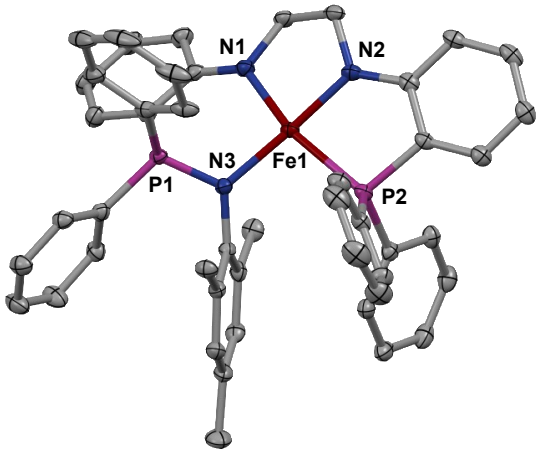

Figure 2: Displacement ellipsoid (50%) representation of **2**. All H atoms and the diethyl ether solvate molecule are omitted for clarity. Relevant geometric parameters (distances in Å, angles in °): Fe1–N1: 1.9659(18), Fe1–N2: 1.8984(17), Fe1–N3: 1.9683(17), Fe1–P2: 2.2856(6), P1–N3: 1.6201(17), N1–Fe1–P2: 163.22(5), N2–Fe1–N3: 172.61(7), τ_4 = 0.171.

Since the net oxidation process is phosphorus-based, the Fe^{II} oxidation state is maintained, as supported by zero-field ^{57}Fe Mössbauer spectroscopy measurements (Figure S2 and Table 1). The isomer shift (δ) observed for **2** is 0.46 mm/s, which is substantially higher than the previously reported isomer shifts for S = 1 Fe^{II} complex **1** (δ = 0.17 mm/s)[30] and its S = 0 Fe^{II} Si–H and B–H activation products (δ = 0.16–0.24 mm/s).[30,33] The increase in isomer shift from **1** to **2** may be explained by the increased *d* electron density afforded by replacement of one of the π-accepting phosphines by a π-donating phosphinimine (as observed, for example, in the series of complexes examined by Neese).[34] Although the spin state of **2** cannot be unequivocally assigned using Mössbauer spectroscopy alone, the solution-state magnetic moment of **2** was found to be 3.63 μ_B, which is most consistent with maintenance of the S = 1 spin state. Although 3.63 μ_B is higher than the spin-only value of 2.83 μ_B expected for S = 1 species, it is consistent with other square planar S = 1 iron species, including **1**.[30,35–38] On this basis, we assign **2** as an intermediate-spin S = 1 Fe^{II} complex.

Treatment of **1** with 2.5 equiv of $MesN_3$ (Scheme 1) in C_6H_6 resulted in a dramatic color change from the deep red-brown typical of **1** to a dark yellow-green. The ^{1}H NMR spectrum of the product revealed a symmetric species **3**, as evident by the appearance of just eight broad and paramagnetically shifted peaks, roughly half the number compared to **2**. Based on the stoichiometry and comparisons to **2**, we posited that **3** was the result of oxidation of both phosphine donors of the Fe-bound $[PNNP]^{2-}$ ligand to phosphinimines.

Indeed, the solid-state structure of **3** (Figure 3) revealed that both phosphine donors of the $[PNNP]^{2-}$ ligand have been converted to phosphinimines in **3**. Unlike **2**, the geometry about Fe in **3** is distorted tetrahedral (τ_4 = 0.452). As was the case with **2**, the P–N bond lengths of 1.617(3) and 1.614(3) Å are on the order of a P=N double bond, suggesting that both phosphinimine donors adopt the neutral phosphorus(V) resonance form as L-type ligands. The elongated $Fe–N_{amide}$ bonds in **3** (2.058(3) and 2.055(3) Å) relative to those in **2** (1.966(2) and 1.899(2) Å) and **1** (1.872 Å) as well as the distorted tetrahedral geometry are both suggestive of a high-spin Fe complex.

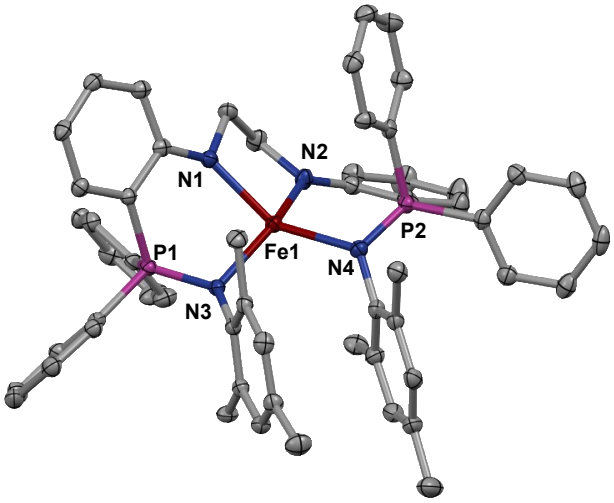

Figure 3: Displacement ellipsoid (50%) representation of **3**. All H atoms and solvent molecules are omitted for clarity. Relevant geometric parameters (distances in Å, angles in °): Fe1–N1: 2.058(3), Fe1–N2: 2.055(3), Fe1–N3: 2.080(3), Fe1–N4: 2.085(3), P1–N3: 1.617(3), P2–N4: 1.614(3), N2–Fe1–N3: 148.45(10), N1–Fe1–N4: 147.78(10) τ_4 = 0.452.

The Fe^{II} oxidation and spin state of **3** were further investigated using zero-field ^{57}Fe Mössbauer spectroscopy (Figure S2 and Table 1). The Mössbauer spectrum of **3** reveals a quadrupole doublet centered at δ = 0.95 mm/s. This isomer shift is significantly increased with respect to **1** and **2** but compares favorably to other high-spin S = 2 Fe^{II} complexes.[39–42] A solution-state magnetic moment measurement afforded a magnetic moment of 5.31 μ_B, which is consistent with the spin-only value (4.90 μ_B) expected for an S = 2 species. This observed change in spin state from S = 1 in **1** and **2** to S = 2 in **3** is likely due to the change in ligand field, as the phosphines in **1** and **2** are expected to be stronger field than phosphinimine ligands. The geometric distortion from square planar toward tetrahedral is also consistent with the proposed S = 2 spin state.

We questioned whether additional mesityl azide would react further with **3** in a metal-centered reaction once both phosphines were oxidized. Treatment of **1** with ⩾ 3 equiv of $MesN_3$ results in the exclusive formation of **3** with unreacted $MesN_3$ observed by ^1H NMR spectroscopy. We propose that this lack of further reactivity can be attributed to steric and electronic differences between **3**, which is S = 2 and tetrahedral with weak field ligands, and **1** and **2,** which are S = 1 and square planar with stronger field ligands.

Table 1: Zero-field ^{57}Fe Mössbauer parameters obtained by fitting spectra obtained at 4 K and effective magnetic moments measured in C_6D_6 solution for Fe-containing compounds **1**-**3**.

	^{57}Fe Mössbauer		μ_{eff}, μ_B
	δ, mm/s	$\lvert\Delta E_Q\rvert$, mm/s	
1[30]	0.17	2.20	3.62
2	0.46	1.96	3.63
3	0.95	1.31	5.31

As organic azides are often used as nitrene transfer reagents to generate high valent iron imido complexes, we hypothesized that the transformation observed herein proceeds through an Fe=NMes intermediate **Int-A** (Scheme 2). No intermediate species were detected when reactions to form **2** or **3** were monitored *in situ* using ^1H NMR spectroscopy. Therefore, we attempted experiments to verify our proposed mechanism and explored the viability and thermodynamic accessibility of intramolecular nitrene transfer

from Fe to P shown, as shown in Scheme 2, using density functional theory (DFT) calculations.

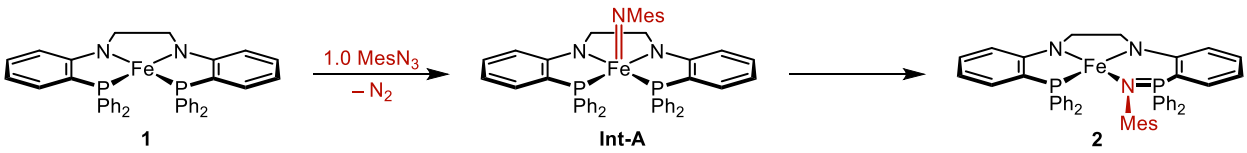

Scheme 2: Proposed mechanism for formation of **2** from **1** through intermediate **Int-A**.

First, we sought to ensure that the phosphinimine is formed by a process involving the Fe center of **1** rather than by a direct Staudinger reaction between the organic azide and the phosphine sidearms. We deemed that such a reaction would be unlikely while the phosphines remain bound to Fe but could be made possible by reversible phosphine dissociation. To this end, we attempted a direct Staudinger reaction of the unmetallated H_2[PNNP] ligand precursor with $MesN_3$ in THF (Scheme 3(a)) and monitored the progress of the reaction by $^{31}P\{^1H\}$ NMR spectroscopy (Figure S3). While we did observe conversion to the phosphinimine, the progress of this reaction was much slower than the conversion of **1** to **2** or **3**. Over the course of 20 h, only ~50% phosphine-to-phosphinimine conversion was noted in the absence of Fe, beyond which point no further conversion was observed. The direct Staudinger reaction pathway is therefore quite slow compared to the 2 h timescale used for the synthesis of **2** and **3**. Since the conversion is accelerated dramatically when ligated to Fe, it is likely that a reaction with the Fe center is responsible for the conversion to the phosphinimine.

We then explored the impact of blocking one of the apical coordination sites on the (PNNP)Fe center. Considering that one of the axial coordination sites of the previously reported five-coordinate (PNNP)Fe(PMe_3) complex[30] is occupied by PMe_3, we investigated whether this would hinder the generation of a phosphinimine-ligated species. Treatment of (PNNP)Fe(PMe_3) with 3 equiv of $MesN_3$ (Scheme 3(b)) resulted in no conversion to **2**, **3**, or any other new iron-containing species after one hour; the ^1H and $^{31}P\{^1H\}$ NMR spectra of the crude reaction mixture (Figures S4 and S5) revealed only the starting materials and small amounts of the Staudinger products originating from reactions with free H_2[PNNP] and PMe_3, likely a result of minor decomposition pathways. This experiment provides further support for the involvement of Fe in the phosphine oxidation process since blocking one of the apical coordination sites of the (PNNP)Fe complex in (PNNP)Fe(PMe_3) may preclude the formation of any Fe-bound intermediates.

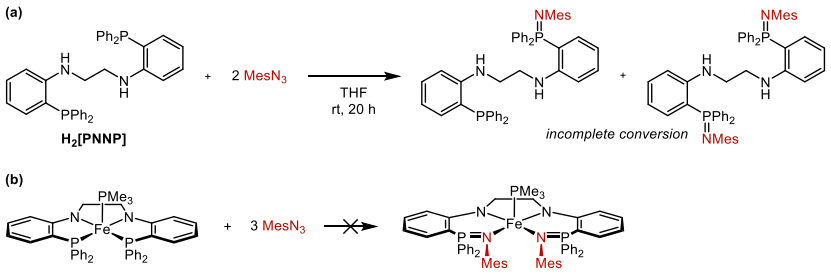

Scheme 3: Mechanistic control experiments. (a) Staudinger reaction of unmetallated H_2PNNP] with mesityl azide. (b) Attempted oxidation of (PNNP)Fe(PMe_3) with mesityl azide.

Finally, we sought to explore the thermodynamic driving force associated with this transformation *in silico*. Since the mechanism for formation of high valent metal-imido species from organic azides is well understood,[43–46] we focused our attention on a potential intramolecular nitrene transfer step from Fe to P. Geometry optimizations of **Int-A** and **2** (both calculated in S = 1 spin states) were performed at the ωB97X-D_3/def2-SVP level of theory using the CPCM solvation model in THF.

The optimized geometry of Fe imido complex **Int-A** was found to be approximately square pyramidal

with the Fe center puckered 0.4 Å out of the tetradentate plane formed by the $[PNNP)]^{2-}$ ligand (Figure 4). Analysis of the spin density surface (Figure 4) and Mulliken spin populations revealed that there is one unpaired electron on the Fe center and another on the N atom of the imido ligand, suggesting that the most appropriate bonding description is that of an Fe^{III}-imidyl radical. The Fe–N_{imidyl} distance is 1.719 Å, which is elongated relative to the Fe–N distance observed in other phosphine-bound iron imido complexes (1.62–1.68 Å) [11,20–26] and similar to the Fe–N distance in a previously reported iron-bound imidyl radical (1.76 Å).[14] The Fe–N–C angle is 138.8°, further supporting the Fe^{III}-imidyl description. All aromatic C=C bonds within the ring of the imidyl ligand are 1.41 ± 0.02 Å, consistent with localization of the radical on the N center rather than delocalization throughout the aromatic system.

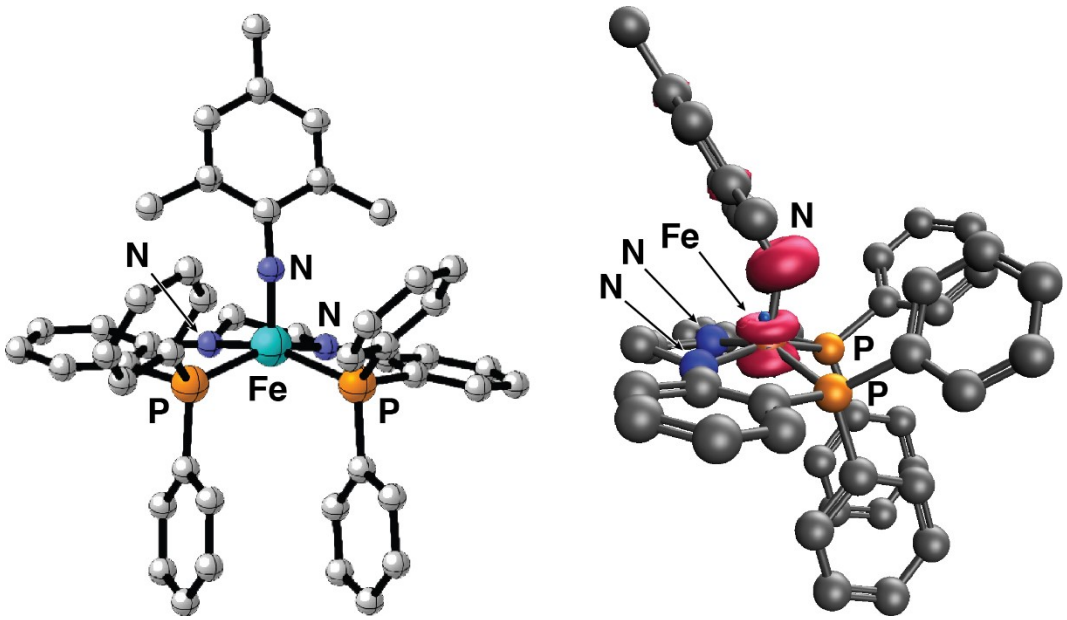

Figure 4: DFT-optimized geometry of **Int-A** (left) and its spin density surface (right). Mulliken spin densities: Fe (0.93), N (0.89).

The driving force for the **Int-A** → **2** transformation was determined to be $\Delta G^\circ = -39.0$ kcal/mol. From this very favorable driving force and the close proximity of the N_{imido} to the phosphine ligands in the square pyramidal environment of **2**, it is unsurprising that any Fe=NR intermediate that is formed would immediately attack the appended P^{III} donor. Presumably, complex **3** is formed via a similar series of downhill steps. Unfortunately, the favorability of intramolecular nitrene transfer to phosphorus limits the synthetic utility of **Int-A** as a potential intermolecular nitrene transfer agent.

Conclusions

In conclusion, we report herein the *in situ* synthesis of two Fe-phosphinimine complexes. Treating **1** with 1 equiv $MesN_3$ produces the asymmetric complex **2**, in which one of the (PNNP) phosphines has been oxidized to a phosphinimine ligand. A reaction between **1** and 2 equiv of $MesN_3$ similarly produces **3**, in which both phosphines are converted to phosphinimines. Investigation of these two complexes by zero-field ^{57}Fe Mössbauer spectroscopy and measurement of their solution magnetic moment confirmed that both **2** and **3** remain in the Fe^{II} oxidation state, but the weaker ligand field afforded by the phosphinimine ligands promotes a transition from the intermediate-spin $S = 1$ state in **1** and **2** to a high-spin $S = 2$ Fe^{II} configuration for **3**. We posited that this transformation proceeds through a putative Fe=NMes intermediate. Although we were unable to observe such an intermediate spectroscopically, we noted that the phosphinimines are not formed when the open coordination sites of **1** are blocked, suggesting that the Fe center is instrumental in the formation of the phosphinimines. We also showed that conversion to the phosphinimine when ligated to Fe is considerably faster than the direct Staudinger reaction between the unligated H_2[PNNP] ligand and $MesN_3$. Finally, we also investigated the viability of an Fe=NR intermediate, finding that such a species is best described as an Fe^{III}-imidyl complex. As expected, the phosphinimine product was found to be thermodynamically downhill with respect to the Fe^{III}-imidyl.

Experimental Details

General Considerations

Unless otherwise noted, all manipulations were carried out under an inert atmosphere using a nitrogen-filled glovebox or standard Schlenk techniques. Glassware was oven-dried before use. Solvents were degassed by sparging with ultra-high purity argon and dried via passage through columns of drying agents using a Glass Contours solvent purification system from Pure Process Technologies. Benzene-d_6 was degassed via repeated freeze-pump-thaw cycles and dried over 3 Å molecular sieves before use. (PNNP)Fe (**1**),[30] H_2[PNNP],[47] mesityl azide,[48] and (PNNP)Fe(PMe_3)[30] were prepared according to literature procedures. NMR spectra were recorded at ambient temperature unless otherwise stated on a Bruker DPX 400 MHz spectrometer. ^{1}H NMR chemical shifts were referenced to residual solvent resonances and are reported in ppm. ^{31}P{^{1}H} NMR chemical shifts were referenced to an external standard of 85% phosphoric acid (0 ppm) and are reported in ppm. Effective magnetic moments (μ_{eff}) were measured using Evans' NMR method.[49]

*Synthesis of (PNNP=NMes)Fe (**2**)*

To a 20 mL scintillation vial equipped with a stir bar, **1** (0.0402 g, 0.0633 mmol) was dissolved in C_6H_6 (3 mL). A C_6H_6 (1 mL) solution of mesityl azide (0.0102 g, 0.0633 mmol, 1.0 equiv) was added dropwise. The mixture was allowed to stir for 80 minutes, during which time the solution changed from a deep red-brown to a dark orange color. The volatile components were removed in vacuo via lyophilization. Single crystals suitable for X-ray diffraction analyses were grown by vapor diffusion of Et_2O into a concentrated THF solution of **2** at –35°C. Collection of these orange crystals yielded **2** as a spectroscopically pure solid (0.0289 g, 58.4%). ^{1}H NMR (400 MHz, C_6D_6): δ 34.86, 26.96, 24.03, 20.44, 19.21, 10.76, 7.66, 7.43, 6.82, 3.71, 2.20, 0.78, –3.72, –18.45, –25.52, –26.10, –58.70. All peaks are broad singlets owing to the paramagnetism of **2**. Evans' method (C_6D_6): 3.63 μ_B. Combustion analysis data were not obtained owing to the air and moisture sensitivity of **2** and its thorough characterization using alternative methods including ^{1}H NMR and zero-field ^{57}Fe Mössbauer spectroscopies.

*Synthesis of (MesN=PNNP=NMes)Fe (**3**)*

To a 20 mL scintillation vial equipped with a stir bar, **1** (0.0753 g, 0.119 mmol) was dissolved in C_6H_6 (3 mL). A C_6H_6 (1 mL) solution of mesityl azide (0.0496 g, 0.308 mmol, 2.6 equiv) was added dropwise. The mixture was allowed to stir for 120 minutes, during which time the solution changed from a deep red-brown to a dark yellow-green color. The volatile components were removed in vacuo via lyophilization. Single crystals suitable for X-ray diffraction analyses were grown by vapor diffusion of Et_2O into THF in the glovebox

freezer at –35°C. Collection of these yellow-green crystals yielded **3** as a spectroscopically pure solid (0.0262 g, 23.7%). ^{1}H NMR (400 MHz, C_6D_6): δ 44.75, 41.87, 26.13, 2.11, 1.35, 0.30, —23.59, —26.09. All peaks are broad singlets owing to the paramagnetism of **3**. Evans' method (C_6D_6): 5.31 μ_B. Combustion analysis data were not obtained owing to the air and moisture sensitivity of **3** and its thorough characterization using alternative methods including ^{1}H NMR and zero-field ^{57}Fe Mössbauer spectroscopies.

Attempted Reaction of (PNNP)Fe(PMe$_3$) with Mesityl Azide

To a 20 mL scintillation vial containing (PNNP)Fe(PMe$_3$) (0.010 g, 0.015 mmol) in THF (2 mL), a solution of mesityl azide (0.008 g, 0.047 mmol, 3 equiv) in THF was added. The solution was allowed to stir for 1 h. Volatiles were removed in vacuo to yield a red powder. The only observed products from this control reaction were unreacted (PNNP)Fe(PMe$_3$) and MesN$_3$, with a small amount of free ligand that dissociated and reacted with the azide via the Staudinger reaction.

Attempted Reaction of H$_2$[PNNP] with Mesityl Azide

To a 50-mL round bottom flask (open to atmosphere), H$_2$[PNNP] (54.6 mg, 0.094 mmol) and THF (3 mL) were added and stirred for 10 min to ensure complete dissolution of the H$_2$[PNNP] . Mesityl azide (30.6 mg, 0.19 mmol, 2.02 equiv) was added to the stirring solution, using a portion of THF (1 mL) to rinse the reagent vial to ensure quantitative transfer. The mixture was allowed to stir for 20 h. Aliquots were taken at 1, 2, 3, 4, 5, and 20 h marks and analyzed by ^{31}P{^{1}H} NMR to monitor conversion. Only ~50% oxidation of the phosphine moieties to the phosphinimines (assigned based on ^{31}P{^{1}H} NMR spectra) was noted over the 20 h period. Additional time did not result in further conversion.

Mössbauer Spectroscopy Details

Samples for zero-field ^{57}Fe Mössbauer spectroscopy were prepared by suspending approximately 30 mg of sample in Paratone®-N cryoprotectant oil and loaded into the sample holder under liquid N_2. Spectra were obtained at $\leqslant$4 K over a 24-hour period using a See Co. (Minneapolis, MN) constant-acceleration spectrometer equipped with a Janis SHI-4 cryostat. Isomer shifts (δ) are reported relative to a 25-μm thick sample of α-Fe foil at 295 K. Data folding and fitting routines were performed using the WMOSS-4F software package.[50]

*Single-Crystal X-Ray Diffraction Data Collection, Solution, and Refinement of **2***

The single crystal X-ray diffraction studies were carried out on a Nonius Kappa Apex II diffractometer equipped with Mo K_α radiation (λ = 0.71073 Å). The crystal was mounted on a MiTeGen Micromount with Paratone 24EX oil. Data were collected in a nitrogen gas stream at 100(2) K using ϕ and ω scans. Data collection was 99.8% complete to 25°in θ (0.83 Å). The crystal-to-detector distance was 60 mm using variable exposure time (4 s to 10 s) depending on θ with a scan width of 1.0°. A total of 150059 reflections were collected with $-13 \leqslant h \leqslant 13$, $-15 \leqslant k \leqslant 15$, $-24 \leqslant l \leqslant 24$. Of these, 9449 reflections were found to be symmetry independent, with a R_{int} of 0.0259. Indexing and unit cell refinement indicated a primitive triclinic lattice with space group P1. The data were integrated using the Bruker SAINT[51] software program and scaled using the SADABS[52] software program. Structure solution and refinement were done within the Olex2 software package.[53] Solution by direct methods (SHELXT[54]) produced a complete phasing model for refinement. All nonhydrogen atoms were refined anisotropically by full-matrix least-squares (SHELXL-2014[55]). All hydrogen atoms were placed using a riding model with positions constrained relative to their parent atom using the appropriate HFIX command in SHELXL-2014. A summary of determined parameters and refinement statistics are available in Table S1.

*Single-Crystal X-Ray Diffraction Data Collection, Solution, and Refinement of **3***

The single crystal X-ray diffraction studies were carried out on a Nonius Kappa Apex II diffractometer equipped with Mo K_α radiation (λ = 0.71073 Å). The crystal was mounted on a MiTeGen Micromount with Paratone 24EX oil. Data were collected in a nitrogen gas stream at 100(2) K using ϕ and ω scans. Data collection was 99.8% complete to 25° in θ (0.83 Å). The crystal-to-detector distance was 60 mm using variable exposure time (4 s to 10 s) depending on θ with a scan width of 1.0°. A total of 136191 reflections

were collected with $-56 \leqslant h \leqslant 56$, $-19 \leqslant k \leqslant 19$,$-17 \leqslant l \leqslant 17$. Of these, 10154 reflections were found to be symmetry independent, with a R_{int} of 0.0794. Indexing and unit cell refinement indicated a C-centered monoclinic lattice with space group C2/c. The data were integrated using the Bruker SAINT[51] software program and scaled using the SADABS[52] software program. Structure solution and refinement were done within the Olex2 software package.[53] Solution by direct methods (SHELXT[54]) produced a complete phasing model for refinement. All nonhydrogen atoms were refined anisotropically by full-matrix least-squares (SHELXL-2014[55]). All hydrogen atoms were placed using a riding model with positions constrained relative to their parent atom using the appropriate HFIX command in SHELXL-2014. A summary of determined parameters and refinement statistics are available in Table S1.

Computational Details

All calculations were performed in the ORCA 5.0.4 software package[56,57] and accounted for solvation effects in THF (ϵ = 7.25; n = 1.407) using the CPCM model[58]. Geometry optimizations for all complexes were performed at the ωB97X-D_3[59] / def2-SVP[60] level of theory. Crystallographic coordinates were used as the input geometries for products **2** and **3** or were used as a starting point and modified as necessary for intermediates whose crystallographic coordinates were not available. In all cases, ORCA-internal basis sets, which include appropriate pseudopotentials as necessary, were employed without modification. The natures of the resulting stationary states were verified by performing single-point frequency calculations on the optimized geometries. For structures in which imaginary frequencies were identified, a small structural perturbation along the negative dimension of the Hessian was applied before a subsequent reoptimization to resolve the imaginary frequency. All free energies herein are reported with solvation effects included.

Acknowledgements
This material was supported by the National Science Foundation under Grant CHE-2101002. The authors are grateful for access to the Ohio Supercomputer Center.[61]

Appendix A. Supplementary data

CCDC 2307664–2307665 contains the supplementary crystallographic data for compounds **2** and **3**. These data can be obtained free of charge via http://www.ccdc.cam.ac.uk/conts/retrieving. html, or from the Cambridge Crystallographic Data Centre, 12 Union Road, Cambridge CB2 1EZ, UK; fax: (+44) 1223-336-033; or e-mail: deposit@ccdc.cam.ac.uk. Supplementary data to this article can be found online at https://doi.org/_____.

References

[1] J.F. Berry, Terminal Nitrido and Imido Complexes of the Late Transition Metals, Comments Inorg. Chem. 30 (2009) 28–66. https://doi.org/10.1080/02603590902768875.
[2] T. R. Cundari, Transition metal imido complexes, J. Am. Chem. Soc. 114 (2002) 7879–7888. https://doi.org/10.1021/ja00046a037.
[3] M.P. Mehn, J.C. Peters, Mid- to high-valent imido and nitrido complexes of iron, J. Inorg. Biochem. 100 (2006) 634–643. https://doi.org/10.1016/j.jinorgbio.2006.01.023.
[4] C.T. Saouma, J.C. Peters, M≡E and M=E complexes of iron and cobalt that emphasize three-fold symmetry (E = O, N, NR), Coord. Chem. Rev. 255 (2011) 920–937. https://doi.org/10.1016/j.ccr.2011.01.009.
[5] J.J. Scepaniak, J.A. Young, R.P. Bontchev, J.M. Smith, Formation of Ammonia from an Iron Nitrido Complex, Angew. Chem. Int. Ed. 48 (2009) 3158–3160. https://doi.org/10.1002/anie.200900381.
[6] G. Ertl, Elementary Steps in Heterogeneous Catalysis, Angew. Chem. Int. Ed. . 29 (1990) 1219–1227. https://doi.org/10.1002/anie.199012191.
[7] J. Hohenberger, K. Ray, K. Meyer, The biology and chemistry of high-valent iron-oxo and iron-nitrido complexes, Nat Commun. 3 (2012) 720. https://doi.org/http://dx.doi.org/10.1038/ncomms1718.
[8] J.L. Crossland, D.R. Tyler, Iron–dinitrogen coordination chemistry: Dinitrogen activation and reactivity, Coord. Chem. Rev. 254 (2010) 1883–1894. https://doi.org/10.1016/j.ccr.2010.01.005.
[9] R.E. Cowley, P.L. Holland, C–H activation by a terminal imidoiron(III) complex to form a cyclopentadienyliron(II) product, Inorganica Chim. Acta. 369 (2011) 40–44. https://doi.org/10.1016/j.ica.2010.11.031.

[10] R. E. Cowley, N. A. Eckert, S. Vaddadi, T. M. Figg, T. R. Cundari, P. L. Holland, Selectivity and Mechanism of Hydrogen Atom Transfer by an Isolable Imidoiron(III) Complex, J. Am. Chem. Soc. 133 (2011) 9796–9811. https://doi.org/10.1021/ja2005303.
[11] J. Cheng, J. Liu, X. Leng, T. Lohmiller, A. Schnegg, E. Bill, S. Ye, L. Deng, A Two-Coordinate Iron(II) Imido Complex with NHC Ligation: Synthesis, Characterization, and Its Diversified Reactivity of Nitrene Transfer and C–H Bond Activation, Inorg. Chem. 58 (2019) 7634–7644. https://doi.org/10.1021/acs.inorgchem.9b01147.
[12] I. Nieto, F. Ding, R.P. Bontchev, H. Wang, J.M. Smith, Thermodynamics of Hydrogen Atom Transfer to a High-Valent Iron Imido Complex, J. Am. Chem. Soc. 130 (2008) 2716–2717. https://doi.org/10.1021/ja0776834.
[13] R.E. Cowley, N.A. Eckert, J. Elhaik, P.L. Holland, Catalytic nitrene transfer from an imidoiron(iii) complex to form carbodiimides and isocyanates, Chem. Commun. (2009) 1760–1762. https://doi.org/10.1039/B820620A.
[14] D. A. Iovan, T. A. Betley, Characterization of Iron-Imido Species Relevant for N-Group Transfer Chemistry, J. Am. Chem. Soc. 138 (2016) 1983–1993. https://doi.org/10.1021/jacs.5b12582.
[15] C. A. Richards, N. P. Rath, J. M. Neely, Isolation and Reactivity of an Iron Azametallacyclobutene Complex, Organometallics. 41 (2022) 1763–1768. https://doi.org/10.1021/acs.organomet.2c00151.
[16] M. J. T. Wilding, D. A. Iovan, T. A. Betley, High-Spin Iron Imido Complexes Competent for C–H Bond Amination, J. Am. Chem. Soc. 139 (2017) 12043–12049. https://doi.org/10.1021/jacs.7b06682.
[17] J.W.W. Chang, T.M.U. Ton, P.W.H. Chan, Transition-metal-catalyzed aminations and aziridinations of C-H and C-C bonds with iminoiodinanes, Chem. Rec. 11 (2011) 331–357. https://doi.org/10.1002/tcr.201100018.
[18] C. A. Richards, N. P. Rath, J. M. Neely, Iron-Catalyzed Alkyne Carboamination via an Isolable Iron Imide Complex, Organometallics. 40 (2021) 2945–2950. https://doi.org/10.1021/acs.organomet.1c00454.
[19] Y. Gao, X. Li, J. E. Stevens, H. Tang, J. M. Smith, Catalytic 1,3-Proton Transfer in Alkenes Enabled by Fe═NR Bond Cooperativity: A Strategy for pKa-Dictated Regioselective Transposition of C═C Double Bonds, J. Am. Chem. Soc. 145 (2023) 11978–11987. https://doi.org/10.1021/jacs.2c13350.
[20] S.D. Brown, T.A. Betley, J.C. Peters, A Low-Spin d5 Iron Imide: Nitrene Capture by Low-Coordinate Iron(I) Provides the 4-Coordinate Fe(III) Complex [PhB(CH2PPh2)3]Fe≡N-p-tolyl, J. Am. Chem. Soc. 125 (2003) 322–323. https://doi.org/10.1021/ja028448i.
[21] S. Kuppuswamy, T.M. Powers, B.M. Johnson, M.W. Bezpalko, C.K. Brozek, B.M. Foxman, L.A. Berben, C.M. Thomas, Metal-Metal Interactions in C_3-Symmetric Diiron Imido Complexes Linked by Phosphinoamide Ligands, Inorg. Chem. 52 (2013) 4802–4811. https://doi.org/10.1021/ic302108k.
[22] T.A. Betley, J.C. Peters, Dinitrogen Chemistry from Trigonally Coordinated Iron and Cobalt Platforms, J. Am. Chem. Soc. 125 (2003) 10782–10783. https://doi.org/doi:10.1021/ja036687f.
[23] C.M. Thomas, N.P. Mankad, J.C. Peters, Characterization of the Terminal Iron(IV) Imides {[PhBPtBu2(pz')]FeIV=NAd}+, J. Am. Chem. Soc. 128 (2006) 4956–4957. https://doi.org/10.1021/ja0604358.
[24] K.E. Aldrich, B. Scott Fales, A. K. Singh, R. J. Staples, B. G. Levine, J. McCracken, M. R. Smith III, A. L. Odom, Electronic and Structural Comparisons between Iron(II/III) and Ruthenium(II/III) Imide Analogs, Inorg. Chem. 58 (2019) 11699–11715. https://doi.org/10.1021/acs.inorgchem.9b01672.
[25] S.D. Brown, J.C. Peters, Ground-State Singlet L3Fe-(μ-N)-FeL_3 and L_3Fe(NR) Complexes Featuring Pseudotetrahedral Fe(II) Centers, J. Am. Chem. Soc. 127 (2005) 1913–1923. https://doi.org/10.1021/ja0453073.
[26] M.-E. Moret, J.C. Peters, Terminal Iron Dinitrogen and Iron Imide Complexes Supported by a Tris(phosphino)borane Ligand, Angew. Chem. Int. Ed. 50 (2011) 2063–2067. https://doi.org/10.1002/anie.201006918.
[27] A. Buchard, B. Komly, A. Auffrant, X. F. Le Goff, P. Le Floch, A Mixed Phosphine−Iminophosphorane Tetradentate Ligand: Synthesis, Coordination to Group 10 Metal Centers, and Use as Catalyst in Suzuki−Miyaura Coupling, Organometallics. 27 (2008) 4380–

4385. https://doi.org/10.1021/om8002637.
[28] J. Xiao, L. Deng, Iron-mediated C–H bond amination by organic azides on a tripodal bis(anilido)iminophosphorane platform, Dalton Trans. 42 (2013) 5607–5610. https://doi.org/10.1039/C3DT50518A.
[29] D. Taher, J.R. Wilson, G. Ritch, M. Zeller, N.K. Szymczak, Late-stage ligand functionalization via the Staudinger reaction using phosphine-appended 2,2′-bipyridine, Chem. Commun. 57 (2021) 5718–5721. https://doi.org/10.1039/D1CC01407B.
[30] G.P. Hatzis, C.M. Thomas, Metal-ligand cooperativity across two sites of a square planar iron(II) complex ligated by a tetradentate PNNP ligand, Chem. Commun. 56 (2020) 8611–8614. https://doi.org/10.1039/D0CC02152K.
[31] L. Yang, D.R. Powell, R.P. Houser, Structural variation in copper(I) complexes with pyridylmethylamide ligands: structural analysis with a new four-coordinate geometry index, τ4, Dalton Trans. (2007) 955–964. https://doi.org/10.1039/B617136B.
[32] C.R. Groom, I.J. Bruno, M.P. Lightfoot, S.C. Ward, The Cambridge Structural Database, Acta Crystallogr., Sect. B. 72 (2016) 171–179. https://doi.org/10.1107/S2052520616003954.
[33] J.E. Stevens, C.E. Moore, C.M. Thomas, Si–H Bond Activation and Dehydrogenative Coupling of Silanes across the Iron–Amide Bond of a Bis(amido)bis(phosphine) Iron(II) Complex, J. Am. Chem. Soc. 145 (2023) 794–799. https://doi.org/10.1021/jacs.2c12157.
[34] F. Neese, Prediction and interpretation of the 57Fe isomer shift in Mössbauer spectra by density functional theory, Inorganica Chim. Acta. 337 (2002) 181–192. https://doi.org/10.1016/S0020-1693(02)01031-9.
[35] C. Hu, B. C. Noll, C. E. Schulz, W. Robert Scheidt, Four-Coordinate Iron(II) Porphyrinates: Electronic Configuration Change by Intermolecular Interaction, Inorg. Chem. 46 (2007) 619–621. https://doi.org/10.1021/ic0620182.
[36] S. H. Strauss, M. E. Silver, K. M. Long, R. G. Thompson, R. A. Hudgens, K. Spartalian, J. A. Ibers, Comparison of the molecular and electronic structures of (2,3,7,8,12,13,17,18-octaethylporphyrinato)iron(II) and (trans-7,8-dihydro-2,3,7,8,12,13,17,18-octaethylporphyrinato)iron(II), J. Am. Chem. Soc. 107 (2002) 4207–4215. https://doi.org/10.1021/ja00300a021.
[37] C. Da Silva, L. Bonomo, E. Solari, R. Scopelliti, C. Floriani, N. Re, The binding ability of iron bonded to porphodimethene: Structural, magnetic, and electronic relationship to iron porphyrin complexes, Chem. - A Eur. J. 6 (2000) 4518–4531. https://doi.org/10.1002/1521-3765(20001215)6:24<4518::AID-CHEM4518>3.0.CO;2-E.
[38] E. J. Hawrelak, W. H. Bernskoetter, E. Lobkovsky, G. T. Yee, E. Bill, P. J. Chirik, Square Planar vs Tetrahedral Geometry in Four Coordinate Iron(II) Complexes, Inorg. Chem. 44 (2005) 3103–3111. https://doi.org/10.1021/ic048202+.
[39] S. Suhr, N. Schröter, M. Kleoff, N. Neuman, D. Hunger, R. Walter, C. Lücke, F. Stein, S. Demeshko, H. Liu, H.-U. Reissig, J. van Slageren, B. Sarkar, Spin State in Homoleptic Iron(II) Terpyridine Complexes Influences Mixed Valency and Electrocatalytic CO2 Reduction, Inorg. Chem. 62 (2023) 6375–6386. https://doi.org/10.1021/acs.inorgchem.3c00253.
[40] T. Sato, K. Nishi, S. Iijima, M. Kojima, N. Matsumoto, One-Step and Two-Step Spin-Crossover Iron(II) Complexes of ((2-Methylimidazol-4-yl)methylidene)histamine, Inorg. Chem. 48 (2009) 7211–7229. https://doi.org/10.1021/ic9006197.
[41] H. Hang, B. Fei, X.Q. Chen, M.L. Tong, V. Ksenofontov, I.A. Gural'skiy, X. Bao, Multiple spin phases in a switchable Fe(ii) complex: polymorphism and symmetry breaking effects, J. Mater. Chem. C. 6 (2018) 3352–3361. https://doi.org/10.1039/C7TC05111E.
[42] G.S. Matouzenko, J.-F. Létard, S. Lecocq, A. Bousseksou, L. Capes, L. Salmon, M. Perrin, O. Kahn, A. Collet, Two-Step Spin Crossover in a Mononuclear Compound [Fe(DPEA)(bim)](ClO4)2·0.5 H2O[DPEA = (2-Aminoethyl)bis(2-pyridylmethyl)amine, bim = 2,2-Bisimidazole] − Crystal Structure, Magnetic Properties, Mössbauer Spectroscopy, and Photomagnetic Effects, Eur. J. Inorg. Chem. 2001 (2001) 2935–2945. https://doi.org/10.1002/1099-0682(200111)2001:11<2935::AID-EJIC2935>3.0.CO;2-D.
[43] S. J. Bonyhady, D. E. DeRosha, J. Vela, D. J. Vinyard, R. E. Cowley, B. Q. Mercado, W. W. Brennessel, P. L. Holland, Iron and Cobalt Diazoalkane Complexes Supported by β-Diketiminate Ligands: A Synthetic, Spectroscopic, and Computational Investigation, Inorg. Chem. 57 (2018) 5959–5972. https://doi.org/10.1021/acs.inorgchem.8b00468.

[44] G. Proulx, R.G. Bergman, Synthesis and Structure of a Terminal Metal Azide Complex: An Isolated Intermediate in the Formation of Imidometal Complexes from Organic Azides, J. Am. Chem. Soc. 117 (1995) 6382–6383. https://doi.org/10.1021/ja00128a038.
[45] G. Proulx, R.G. Bergman, Synthesis, Structures, and Kinetics and Mechanism of Decomposition of Terminal Metal Azide Complexes: Isolated Intermediates in the Formation of Imidometal Complexes from Organic Azides, Organometallics. 15 (1996) 684–692. https://doi.org/10.1021/om950796o.
[46] R. Waterman, G.L. Hillhouse, η2-Organoazide Complexes of Nickel and Their Conversion to Terminal Imido Complexes via Dinitrogen Extrusion, J. Am. Chem. Soc. 130 (2008) 12628–12629. https://doi.org/10.1021/ja805530z.
[47] G.S. Day, B. Pan, D.L. Kellenberger, B.M. Foxman, C.M. Thomas, Guilty as Charged: Non-Innocent Behavior by a Pincer Ligand Featuring a Central Cationic Phosphenium Donor, Chem. Commun. 47 (2011) 3634–3636. https://doi.org/10.1039/C0CC05739H.
[48] D.G. Brown, N. Sanguantrakun, B. Schulze, U.S. Schubert, C.P. Berlinguette, Bis(tridentate) Ruthenium–Terpyridine Complexes Featuring Microsecond Excited-State Lifetimes, J. Am. Chem. Soc. 134 (2012) 12354–12357. https://doi.org/10.1021/ja3039536.
[49] D.F. Evans, The Determination of the Paramagnetic Susceptibility of Substances in Solution by Nuclear Magnetic Resonance, J. Chem. Soc. (1959) 2003–2005. https://doi.org/10.1039/jr9590002003.
[50] I. Prisecaru, WMOSS-4F Mossbauer Spectral Analysis Software, (n.d.) www.wmoss.org.
[51] SAINT v. 8.40b, Bruker AXS Inc., Madison, Wisconsin, USA, 2021.
[52] SADABS v. 2016/2, Bruker AXS Inc., Madison, Wisconsin, USA, 2016.
[53] O. V Dolomanov, L.J. Bourhis, R.J. Gildea, J.A.K. Howard, H. Puschmann, OLEX2: a Complete Structure Solution, Refinement and Analysis Program, J. Appl. Crystallogr. 42 (2009) 339–341. https://doi.org/10.1107/S0021889808042726.
[54] G.M. Sheldrick, SHELXT – Integrated Space-Group and Crystal-Structure Determination, Acta Cryst. A71 (2015) 3–8. https://doi.org/10.1107/S2053273314026370.
[55] G.M. Sheldrick, Crystal structure refinement with SHELXL, Acta Crystallogr. Sect. C Struct. Chem. 71 (2015) 3–8. https://doi.org/10.1107/s2053229614024218.
[56] F. Neese, The ORCA program system, WIREs Comput. Mol. Sci. 2 (2012) 73–78. https://doi.org/10.1002/wcms.81.
[57] F. Neese, Software update: The ORCA program system—Version 5.0, WIREs Comput. Mol. Sci. 12 (2022) e1606. https://doi.org/10.1002/wcms.1606.
[58] V. Barone, M. Cossi, Quantum Calculation of Molecular Energies and Energy Gradients in Solution by a Conductor Solvent Model, J. Phys. Chem. A. 102 (1998) 1995–2001. https://doi.org/10.1021/jp9716997.
[59] J.-D. Chai, M. Head-Gordon, Long-range corrected hybrid density functionals with damped atom–atom dispersion corrections, Phys. Chem. Chem. Phys. 10 (2008) 6615–6620. https://doi.org/10.1039/B810189B.
[60] F. Weigend, R. Ahlrichs, Balanced basis sets of split valence, triple zeta valence and quadruple zeta valence quality for H to Rn: Design and assessment of accuracy, Phys. Chem. Chem. Phys. 7 (2005) 3297–3305. https://doi.org/10.1039/B508541A.
[61] Ohio Supercomputer Center, (1987). http://osc.edu/ark:/19495/f5s1ph73.